JPEDAV (2016) 37:308–318
DOI: 10.1007/s11669-016-0458-y
1547-7037 ©ASM International

Phase Equilibria of the Nd-Fe-B Ternary System

G. Fu, J. Wang, M.H. Rong, G.H. Rao, and H.Y. Zhou

(Submitted February 3, 2016; in revised form March 6, 2016; published online March 23, 2016)

Nd-Fe-B-based alloys as sintered $Nd_2Fe_{14}B$-typed permanent magnets have been studied extensively due to their excellent magnetic properties. In this work, the experimental information on the corresponding phase equilibria of the Nd-Fe-B ternary system in the published literature is reviewed first. The key Nd-Fe-B alloys annealed at 873 and 1073 K were then investigated experimentally to determine the phase equilibria of the system using x-ray diffraction technique and scanning electron microscope (SEM) with energy dispersive spectrometry (EDS). The ternary intermetallic compound, $Nd_2Fe_{14}B$ with space group $P4_2/mnm$ as $Nd_2Fe_{14}B$ structure type, $NdFe_4B_4$ with space group Pccn as $RE_{1.11}Fe_4B_4$ structure type and $Nd_5Fe_2B_6$ with space group R $\bar{3}$ m as $Pr_5Co_2B_6$ structure type were confirmed at 873 and 1073 K. The binary intermetallic compound Nd_5Fe_{17} is stable at 873 K, while it was not found at 1073 K. The phase equilibria of the Nd-Fe-B ternary system consists of 14 single-phase regions, 28 two-phase regions and 16 three-phase regions at 873 K, while there are 8 single-phase regions, 14 two-phase regions and 7 three-phase regions at 1073 K except for the B-rich part.

Keywords intermetallic compound, Nd-Fe-B, permanent magnets, phase equilibria

1. Introduction

Since the $Nd_{15}Fe_{77}B_7$ alloy with high energy product (287 kJ/m^3), remanent magnetization (1.23 T) and coercivity (0.96 T) was discovered by Sagawa et al.,[1] sintered Nd-Fe-B permanent magnets have been used widely in many industrial fields, such as voice coil motors for hard disk drives and motors for hybrid/electric vehicles.[2-8] Subsequently, $Nd_{13}Fe_{81}B_6$ alloy with high energy products (403 kJ/m^3) prepared by sintering process was reported.[9] However, the relatively low intrinsic coercivity (μ_0H_c = 1.2 T) and low operating temperature (585 K) of Nd-Fe-B permanent magnets are still practical obstacles in the application of wind power generators and traction motors.[10] The most effective solution of the improvement of the coercivity is the addition of expensive heavy rare earth elements (e.g. Dy, Tb) to Nd-Fe-B magnets.[11-13] For example, $Nd_{13}Dy_2B_6Fe_{bal}$ alloy was studied to be higher coercivity (1.823 T) after sintered at 1243 K for 20 h,[14] while the coercivities of $Nd_{12-x}Dy_3Tb_xFe_{78}B_7$ alloys increase from 1.7 to 2.0 T with increasing Tb content.[15]

G. Fu, School of Material Science and Engineering, Guilin University of Electronic Technology, Guilin 541004, People's Republic of China; and **J. Wang, M.H. Rong, G.H. Rao,** and **H.Y. Zhou,** School of Material Science and Engineering, Guilin University of Electronic Technology, Guilin 541004, People's Republic of China; and Guangxi Key Laboratory of Information Materials, Guilin University of Electronic Technology, Guilin 541004, People's Republic of China. Contact e-mails: wangjiang158@163.com and rgh@guet.edu.cn.

On the other hand, different heat-treatment processes (e.g. sintering, post-sintering and annealing) have a significant influence on the coercivity of Nd-Fe-B permanent magnets.[16,17] The coercivity of Nd-Fe-B magnet increases from 1.464 to 1.671 T by post-sintering annealing.[18] The coercivity of $Nd_{11.7}Pr_{2.8}Fe_{76.9}B_{6.0}Al_{0.5}Cu_{0.1}O_{2.1}$ alloy was measured to be 1.118 T after post-sintering annealed at 873 K for 1 h.[19] The coercivity of (Nd, Pr)$_{29.5}$Dy$_{2.0}$B$_{1.0}$Al$_{0.2}$Co$_{0.8}$Cu$_{0.1}$Fe$_{bal}$ alloy increases from 1.170 to 1.450 T after two annealing processes (1138 K for 2 h/793 K for 4 h).[20]

To better understand the effect of sintered/heat treatment process on magnetic properties of Nd-Fe-B permanent magnets, the information of phase equilibria and crystal structures of intermetallic compounds in the Nd-Fe-B ternary system are indispensable. Therefore, the purpose of the present work was to study phase equilibria of Nd-Fe-B ternary system at 873 and 1073 K using key alloy samples and x-ray diffraction (XRD) and scanning electron microscopy (SEM) with energy dispersive spectrometry (EDS).

2. Literature Information

2.1 The Fe-Nd Binary System

The Fe-Nd phase diagram was reviewed by Massalski[21] and assessed thermodynamically by Zhang et al.[22] In the Fe-Nd binary system, there are α-Fe, γ-Fe, δ-Fe, α-Nd and β-Nd as stable solid solution phases, Nd_2Fe_{17} with Th_2Zn_{17} structure[23] as an intermetallic compound. The Nd-Fe phase diagram was later revised,[24,25] because a new intermetallic compound Nd_5Fe_{17} with $P6_3/mcm$ space group was found to be stable.[26,27] In addition, the intermetallic compound $NdFe_2$ reported by Chaban et al.[5] was not confirmed to be stable.[24-27] Recently, the thermodynamic assessment of the Nd-Fe binary system was performed by Ende et al.,[28] which agrees well with the experimental results.[24]

2.2 The Fe-B Binary System

The Fe-B binary system was studied by Portnoi et al.[29] and then was calculated by Ende et al.[28] According to the experimental information,[29] α-Fe, γ-Fe, δ-Fe, β-B and two intermetallic compounds, FeB and Fe_2B with a narrow homogeneity range (about 1 at.%), as stable compounds exist in Fe-B binary system.

2.3 The Nd-B Binary System

The Nd-B binary phase diagram was reported by Liao et al.[30] and was thermodynamically assessed by Ende et al.[28] There are several stable phase: α-Nd, β-Nd, Nd_2B_5, NdB_4, NdB_6, NdB_{66} and β-B. The binary intermetallic compounds Nd_2B_5 (Sm_2B_5-type) and NdB_4 (ThB_4-type) were found by x-ray diffraction examination of single crystals.[31,32] Storms et al.[33] reported the composition ranges of NdB_6 (CaB_6-type) are 3.41 at.% B at 1600 K and 4.92 at.% B at 2000 K.

The crystal structure information of the stable phases of the binary systems is given in Table 1.

2.4 The Nd-Fe-B Ternary System

The Nd-Fe-B ternary system has been studied extensively, including isothermal sections at different temperatures, vertical sections at different composition conditions and the liquidus projection,[34-39] and then was reviewed by Raghavan[40] and Malfielt et al.,[41] respectively.

As for the isothermal sections of the Nd-Fe-B ternary system, Chaban et al.[5] determined first the phase equilibria at 873 K in the Fe-rich part and at 673 K in Nd-rich part by means of x-ray diffraction and microscopic analysis. Subsequently, partial isothermal sections at 1173 K (Fe-rich), 973 K (Nd-rich),[34,35] 1273 K[36] and at 298 K (room temperature)[37,38] were reported. The solid-liquid equilibria of this ternary system at 1273 K were investigated experimentally by Schneider et al.[36] It is indicated that the two-phase equilibrium, $Fe_2B + Nd_2Fe_{14}B$ (τ_1) is stable at 1273 K. On the other hand, several vertical sections of Nd-Fe-B system were also investigated experimentally.[36,39-43] The four vertical sections (73.3 at.% Fe, 80 at.% Fe, 4 at.% B and at Fe-$Nd_2Fe_{14}B$) were studied by Schneider et al.[36] The experimental results[36] show that the ternary compound $Nd_2Fe_{14}B$ (τ_1) was considered to be incongruent melting, which is at variance with the congruent formation through the investigation of two vertical sections (6 at.% B and Nd_2Fe_{17}-$Nd_8Fe_{27}B_{24}$) reported by Che et al.[39] Three vertical sections of 4 at.% B, 30 at.% Nd and along $Fe_{77}B_{23}$-$Fe_{27}Nd_{73}$ were studied experimentally by Knoch et al.[42] Landgraf et al.[43] measured the vertical sections of 60 at.% Nd up to 20 at.% B. Rogl et al.[41] pointed out that the experimental results[43] at high temperature are not reasonable, because the temperature of the last thermal effect close to Nd-Fe binary system is at 1223 K, which is much less than the corresponding binary liquidus temperature (1427 K).

The liquidus projection of the Nd-Fe-B ternary system was investigated experimentally.[41-43] Knoch et al.[42] confirmed the eutectic reaction, $L \leftrightarrow Nd_2Fe_{14}B$ (τ_1) + $NdFe_4B_4$ (τ_2) + α-Nd, through differential thermal analysis. The liquidus projection was updated by Knoch et al.,[42] because the region of primary crystallization of $Nd_2Fe_{14}B$ (τ_1) is narrower than the previous results reported by Mastsuura et al.[44]

According to the experimental information mentioned above, three ternary intermetallic compounds, $Nd_2Fe_{14}B$ (τ_1), $NdFe_4B_4$ (τ_2) and $Nd_5Fe_2B_6$ (τ_3) are stable in the Nd-Fe-B ternary system. $Nd_2Fe_{14}B$ (τ_1) was denoted as the $Nd_3Fe_{16}B$ by Chaban et al.[5] Herbst et al.[45] determined its crystal structure with space group ($P4_2/mnm$) and lattice parameters (a = 0.8804 nm, c = 1.2205 nm) by means of

Table 1 Crystallographic data of the stable phases in Nd-Fe-B ternary system

			Lattice parameters			
Phase	**Prototype**	**Space group**	**a (nm)**	**b (nm)**	**c (nm)**	**References**
β-B	βB	$R\bar{3}m$	1.0933	…	2.3825	50
eB	FeB	*Pbmn*	0.5506	0.2952	0.4061	41
Fe_2B	Al_2Cu	$P6_3/mcm$	0.5109	…	0.4249	41
α-Fe	W	$Im\bar{3}m$	0.28665	…	…	21
δ-Fe	W	$Im\bar{3}m$	0.29315	…	…	21
γ-Fe	Cu	$Fm\bar{3}m$	0.36467	…	…	21
α-Nd	αLa	$P6_3/mcm$	0.36582	…	1.1800	21
β-Nd	W	$Im\bar{3}m$	0.41300	…	…	21
Nd_2Fe_{17}	Th_2Zn_{17}	$R\bar{3}m$	0.85675	…	1.2443	27
Nd_5Fe_{17}	Nd_5Fe_{17}	$P6_3/mcm$	2.2148	…	1.2330	26,27
Nd_2B_5	Sm_2B_5	$P2_1/c$	1.50818	0.7252	0.7284	32
NdB_4	ThB_4	$P4/bmb$	0.7219	…	0.4102	31,32
NdB_6	CaB_6	$Pm\bar{3}m$	0.4110	…	…	32
NdB_{66}	ThB_{66}	$Fm\bar{3}c$	2.3500	…	…	32
$Nd_2Fe_{14}B(\tau_1)$	$Nd_2Fe_{14}B$	$P4_2/mnm$	0.8804	…	1.2205	45
$NdFe_4B_4(\tau_2)$	$RE_{1.11}Fe_4B_4$	*Pccn*	0.7117	…	3.5070	46
$Nd_5Fe_2B_6(\tau_3)$	$Pr_5Co_2B_6$	$R\bar{3}m$	0.5464	…	2.4272	47

Table 2 Experimental results of the Nd-Fe-B alloys annealed at 873 K for 1440 h

		Measured composition (at.%) by EDS*			
Number	Nominal composition (at.%)	Nd	Fe	Phase**	Identified phases by XRD
1	$Nd_{15}Fe_{82.5}B_{2.5}$	11.23	88.77	Nd_2Fe_{17}	$Nd_2Fe_{14}B$, Nd_2Fe_{17}, Nd_5Fe_{17}
		20.13	79.87	Nd_5Fe_{17}	
		13.24	86.76	$Nd_2Fe_{14}B$	
2	$Nd_{25}Fe_{72.5}B_{2.5}$	20.13	79.87	Nd_5Fe_{17}	$Nd_2Fe_{14}B$, α-Nd , Nd_5Fe_{17}
		98.12	1.88	α-Nd	
		14.35	85.65	$Nd_2Fe_{14}B$	
3	$Nd_{7.5}Fe_{90}B_{2.5}$	1.58	98.42	α-Fe	$Nd_2Fe_{14}B$, α-Fe, Nd_2Fe_{17}
		14.21	85.79	$Nd_2Fe_{14}B$	
		13.21	86.79	Nd_2Fe_{17}	
4	$Nd_5Fe_{85}B_{10}$	23.58	76.42	$NdFe_4B_4$	α-Fe, $Nd_2Fe_{14}B$, $NdFe_4B_4$
		0.69	99.31	α-Fe	
		15.31	84.69	$Nd_2Fe_{14}B$	
5	$Nd_{10}Fe_{75}B_{15}$	1.31	99.69	α-Fe	α-Fe, $Nd_2Fe_{14}B$, $NdFe_4B_4$
		14.45	85.55	$Nd_2Fe_{14}B$	
		24.25	75.75	$NdFe_4B_4$	
6	$Nd_{15}Fe_{70}B_{15}$	14.21	85.79	$Nd_2Fe_{14}B$	$Nd_2Fe_{14}B$, $NdFe_4B_4$, α-Nd
		99.12	0.88	α-Nd	
		24.52	75.48	$NdFe_4B_4$	
7	$Nd_{25}Fe_{60}B_{15}$	15.11	84.89	$Nd_2Fe_{14}B$	$Nd_2Fe_{14}B$, $NdFe_4B_4$, α-Nd
		99.82	0.18	α-Nd	
		22.21	77.79	$NdFe_4B_4$	
8	$Nd_{45}Fe_{40}B_{15}$	13.98	86.02	$Nd_2Fe_{14}B$	$Nd_2Fe_{14}B$, $NdFe_4B_4$, α-Nd
		99.76	0.24	α-Nd	
		23.22	76.78	$NdFe_4B_4$	
9	$Nd_{20}Fe_{45}B_{35}$	14.56	85.44	$Nd_2Fe_{14}B$	$Nd_2Fe_{14}B$, $NdFe_4B_4$, α-Nd
		99.92	0.08	α-Nd	
		22.41	77.59	$NdFe_4B_4$	
10	$Nd_{65}Fe_{20}B_{15}$	14.52	85.48	$Nd_2Fe_{14}B$	$Nd_2Fe_{14}B$,$NdFe_4B_4$, α-Nd
		99.79	0.21	α-Nd	
		25.12	74.88	$NdFe_4B_4$	
11	$Nd_{42}Fe_{18}B_{40}$	25.31	74.69	$NdFe_4B_4$	α-Nd, $Nd_5Fe_2B_6$, $NdFe_4B_4$
		99.93	0.07	α-Nd	
		74.45	25.55	$Nd_5Fe_2B_6$	
12	$Nd_{78}Fe_7B_{15}$	24.23	75.77	$NdFe_4B_4$	α-Nd, $Nd_5Fe_2B_6$,$NdFe_4B_4$
		99.84	0.16	α-Nd	
		72.35	27.65	$Nd_5Fe_2B_6$	
13	$Nd_{48}Fe_{20}B_{32}$	25.28	74.72	$NdFe_4B_4$	α-Nd, $Nd_5Fe_2B_6$, $NdFe_4B_4$
		98.99	1.01	α-Nd	
		74.32	25.68	$Nd_5Fe_2B_6$	
14	$Nd_{28}Fe_{30}B_{42}$	24.21	75.79	$NdFe_4B_4$	α-Nd, $Nd_5Fe_2B_6$, $NdFe_4B_4$
		98.89	1.11	α-Nd	
		74.53	25.47	$Nd_5Fe_2B_6$	
15	$Nd_{40}Fe_{10}B_{50}$	70.16	29.84	$Nd_5Fe_2B_6$	$Nd_5Fe_2B_6$, Nd_2B_5, α-Nd
		99.85	0.15	α-Nd	
16	$Nd_{75}Fe_5B_{20}$	71.32	28.68	$Nd_5Fe_2B_6$	α-Nd, $Nd_5Fe_2B_6$, Nd_2B_5
		99.88	0.12	α-Nd	
17	$Nd_{35}Fe_5B_{60}$	78.39	21.61	$Nd_5Fe_2B_6$	α-Nd, $Nd_5Fe_2B_6$, Nd_2B_5
		99.88	0.12	α-Nd	
18	$Nd_{59}Fe_5B_{36}$	70.56	29.44	$Nd_5Fe_2B_6$	α-Nd, $Nd_5Fe_2B_6$, Nd_2B_5
		99.15	0.85	α-Nd	
19	$Nd_{50}Fe_5B_{45}$	69.87	30.13	$Nd_5Fe_2B_6$	α-Nd, $Nd_5Fe_2B_6$, Nd_2B_5
		99.97	0.03	α-Nd	

Table 2 continued

Number	Nominal composition (at.%)	Measured composition (at.%) by EDS*			Identified phases by XRD
		Nd	Fe	Phase**	
20	$Nd_{2.5}Fe_{55.5}B_{22}$	23.52	76.48	$NdFe_4B_4$	Fe_2B, $NdFe_4B_4$, α-Fe
		0.22	99.78	α-Fe	
21	$Nd_5Fe_{67}B_{33}$	22.72	77.28	$NdFe_4B_4$	α-Fe, $NdFe_4B_4$, Fe_2B
		99.57	0.43	α-Fe	
22	$Nd_{20}Fe_{20}B_{60}$	73.21	26.79	$Nd_5Fe_2B_6$	$Nd_5Fe_2B_6$, $NdFe_4B_4$, NdB_4
		18.54	81.46	$NdFe_4B_4$	
23	$Nd_{15}Fe_{35}B_{50}$	69.78	30.22	$Nd_5Fe_2B_6$	$Nd_5Fe_2B_6$, $NdFe_4B_4$, NdB_4
		22.14	77.86	$NdFe_4B_4$	
24	$Nd_{15}Fe_{20}B_{65}$	20.88	79.12	$NdFe_4B_4$	Fe_2B, NdB_4, $NdFe_4B_4$
25	$Nd_{30}Fe_5B_{65}$	69.35	30.65	$Nd_5Fe_2B_6$	$Nd_5Fe_2B_6$, Nd_2B_5, NdB_4
26	$Nd_{27.5}Fe_{2.5}B_{70}$	68.18	31.82	$Nd_5Fe_2B_6$	NdB_4, Nd_2B_5, $Nd_5Fe_2B_6$
27	$Nd_7Fe_{48}B_{45}$	21.49	78.51	$NdFe_4B_4$	Fe_2B, $NdFe_4B_4$, NdB_4
28	$Nd_{10}Fe_{20}B_{70}$	…			NdB_6, FeB, NdB_4
29	$Nd_{2.5}Fe_{32.5}B_{65}$	…			NdB_6, FeB, NdB_{66}
30	$Nd_{2.5}Fe_{27.5}B_{70}$	…			NdB_6, FeB, NdB_{66}
31	$Nd_{2.5}Fe_{52.5}B_{45}$	…			Fe_2B, FeB, NdB_4
32	$Nd_{10}Fe_{30}B_{60}$	…			Fe_2B, FeB, NdB_4
33	$Nd_{7.5}Fe_{30}B_{62.5}$	…			NdB_6, FeB, NdB_4

*The compositions of Nd and Fe in Nd-Fe-B alloys measured were shown, while that of B was not given because B as the light element could not accurately measured quantitatively by EDS

**The ternary intermetallic compounds in Nd-Fe-B alloys were identified on the basis of the composition measured of Nd and Fe without any content of B by EDS and XRD analysis

Table 3 Experimental results of the Nd-Fe-B alloys annealed at 1073 K for 960 h

Number	Nominal composition (at.%)	Measured composition (at.%) by EDS*			Identified phases by XRD
		Nd	Fe	Phase**	
1	$Nd_{15}Fe_{82.5}B_{2.5}$	10.25	89.75	Nd_2Fe_{17}	$Nd_2Fe_{14}B$, Nd_2Fe_{17}, α-Nd
		13.52	86.48	$Nd_2Fe_{14}B$	
		99.53	0.47	α-Nd	
2	$Nd_{25}Fe_{72.5}B_{2.5}$	98.51	1.49	α-Nd	$Nd_2Fe_{14}B$, Nd_2Fe_{17}, α-Nd
		14.21	85.79	$Nd_2Fe_{14}B$	
		11.43	88.57	Nd_2Fe_{17}	
3	$Nd_{12}Fe_{85.5}B_{2.5}$	9.65	90.35	Nd_2Fe_{17}	$Nd_2Fe_{14}B$, Nd_2Fe_{17}, α-Nd
		13.54	86.46	$Nd_2Fe_{14}B$	
		98.56	1.44	α-Nd	
4	$Nd_{32.5}Fe_{65}B_{2.5}$	10.51	89.49	Nd_2Fe_{17}	$Nd_2Fe_{14}B$, Nd_2Fe_{17}, α-Nd
		12.98	87.02	$Nd_2Fe_{14}B$	
		99.76	0.24	α-Nd	
5	$Nd_{10}Fe_{75}B_{15}$	2.02	97.98	α-Fe	α-Fe, $Nd_2Fe_{14}B$, $NdFe_4B_4$
		14.05	85.95	$Nd_2Fe_{14}B$	
		23.54	76.46	$NdFe_4B_4$	
6	$Nd_5Fe_{90}B_5$	13.42	86.58	$Nd_2Fe_{14}B$	α-Fe, $Nd_2Fe_{14}B$, $NdFe_4B_4$
		99.22	0.78	α-Nd	
		22.31	77.69	$NdFe_4B_4$	

Table 3 continued

Number	Nominal composition (at.%)	Measured composition (at.%) by EDS*			Identified phases by XRD
		Nd	Fe	Phase**	
7	$Nd_5Fe_{80}B_{15}$	12.97	87.03	$Nd_2Fe_{14}B$	α-Fe, $Nd_2Fe_{14}B$, $NdFe_4B_4$
		0.14	99.86	α-Fe	
		22.19	77.81	$NdFe_4B_4$	
8	$Nd_{15}Fe_{45}B_{40}$	14.02	85.98	$Nd_2Fe_{14}B$	$Nd_2Fe_{14}B$,$NdFe_4B_4$, α-Nd
		99.74	0.26	α-Nd	
		18.52	81.48	$NdFe_4B_4$	
9	$Nd_{15}Fe_{75}B_{10}$	14.18	85.82	$Nd_2Fe_{14}B$	$Nd_2Fe_{14}B$, $NdFe_4B_4$, α-Nd
		97.21	2.79	α-Nd	
		19.49	80.51	$NdFe_4B_4$	
10	$Nd_{45}Fe_{40}B_{15}$	13.84	86.16	$Nd_2Fe_{14}B$	$Nd_2Fe_{14}B$, $NdFe_4B_4$, α-Nd
		98.45	1.55	α-Nd	
		21.43	78.57	$NdFe_4B_4$	
11	$Nd_{25}Fe_{60}B_{15}$	14.11	85.89	$Nd_2Fe_{14}B$	$Nd_2Fe_{14}B$, $NdFe_4B_4$, α-Nd
		98.33	1.67	α-Nd	
		20.43	79.57	$NdFe_4B_4$	
12	$Nd_{40}Fe_{20}B_{40}$	72.12	27.88	$Nd_5Fe_2B_6$	$Nd_5Fe_2B_6$, $NdFe_4B_4$, α-Nd
		97.41	2.59	α-Nd	
		21.12	78.88	$NdFe_4B_4$	
13	$Nd_{28}Fe_{32}B_{40}$	23.67	76.33	$NdFe_4B_4$	$Nd_5Fe_2B_6$, $NdFe_4B_4$, α-Nd
		97.77	2.23	α-Nd	
		73.83	26.17	$Nd_5Fe_2B_6$	
14	$Nd_{7.5}Fe_{90}B_{2.5}$	10.53	89.47	Nd_2Fe_{17}	α-Fe, $Nd_2Fe_{14}B$, Nd_2Fe_{17}
		13.27	86.73	$Nd_2Fe_{14}B$	
		0.66	99.34	α-Fe	
15	$Nd_{65}Fe_5B_{30}$	71.13	28.87	$Nd_5Fe_2B_6$	Nd_2B_5, $Nd_5Fe_2B_6$, α-Nd
		99.68	0.32	α-Nd	
16	$Nd_{47}Fe_5B_{48}$	70.85	29.15	$Nd_5Fe_2B_6$	Nd_2B_5, $Nd_5Fe_2B_6$, α-Nd
		99.74	0.26	α-Nd	
17	$Nd_{2.5}Fe_{85}B_{12.5}$	20.39	79.61	$NdFe_4B_4$	α-Fe, $NdFe_4B_4$, Fe_2B
		0.88	99.12	α-Fe	
18	$Nd_{2.5}Fe_{72.5}B_{25}$	22.16	77.84	$NdFe_4B_4$	α-Fe, $NdFe_4B_4$, Fe_2B
		0.42	99.58	α-Fe	
19	$Nd_5Fe_{65}B_{30}$	23.52	76.48	$NdFe_4B_4$	α-Fe, $NdFe_4B_4$, Fe_2B
		0.79	99.21	α-Fe	

*The compositions of Nd and Fe in Nd-Fe-B alloys measured were shown, while that of B was not given because B as the light element could not accurately measured quantitatively by EDS

**The ternary intermetallic compounds in Nd-Fe-B alloys were identified on the basis of the composition measured of Nd and Fe without any content of B by EDS and XRD analysis

the neutron diffraction. $NdFe_4B_4$ (τ_2) is a nonmagnetic phase found in Nd-Fe-B magnets. Givord et al.[46] studied that its crystal structure is $Nd_{1.11}Fe_4B_4$ structure type with space group (Pccn) and lattice parameters (a = 0.7117 nm, c = 3.5070 nm) through the structure refinement. $Nd_5Fe_2B_6$ (τ_3) with space group (R $\overline{3}$ m) and lattice parameters (a = 0.5460 nm, c = 2.4272 nm) was reported by Buschow et al. [47] through the structure refinement with x-ray data.

Thermodynamic assessment of the Nd-Fe-B ternary system was first performed by Hallenmans et al.,[48] and then was revised by Ende et al.[28] using the quasi-chemical model to describe liquid phase. The invariant reactions in the Nd-Fe-B ternary system were given by Raghavan[49] based on the experimental and calculated results,[28] and a schematic liquidus projection with phases of primary crystallization marked close to the B-rich part was presented.

3. Experimental Procedure

Bulk Nd (99.99% purity), Fe (99.99% purity), B (99.99% purity) and powder Fe (99.99% purity), B (99.999% purity) were used as raw materials. Nd-Fe-B ingots (<60 at.% B) were melted using bulk materials in the arc furnace with a

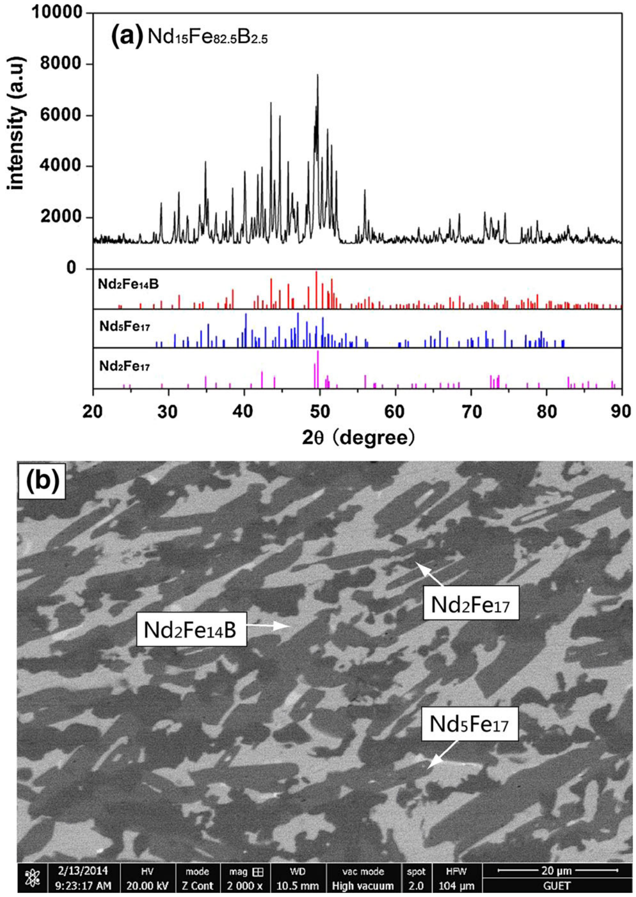

Fig. 1 XRD pattern and backscattered electron image of Nd15Fe82.5B2.5 alloy annealed at 873 K for 1440 h

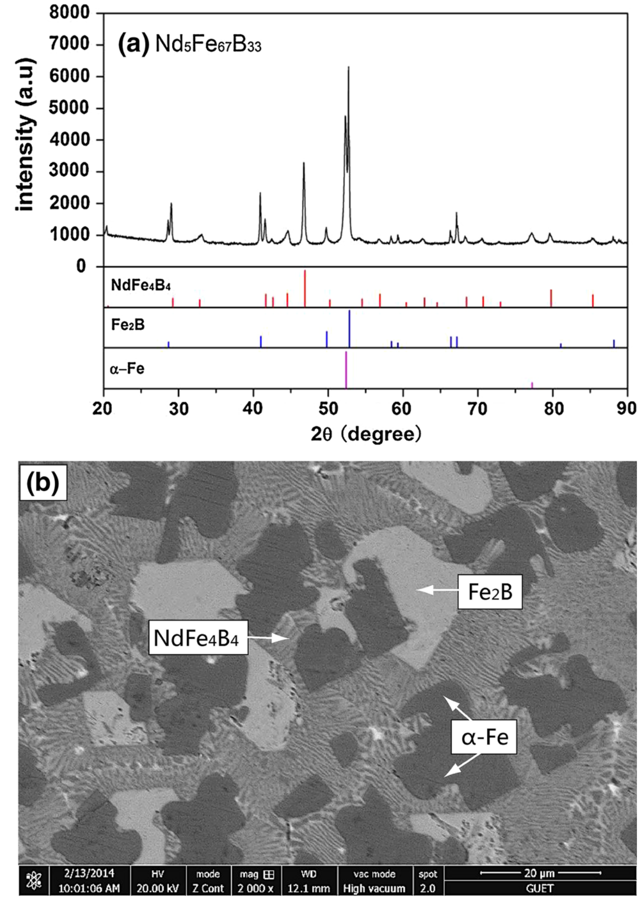

Fig. 2 XRD pattern and backscattered electrons (BSE) image of Nd5Fe67B33 alloy annealed at 873 K for 1440 h

non-consumable tungsten electrode under an inert argon atmosphere. On the other hand, Nd-Fe-B alloys (>60 at.% B) were prepared using powder Fe and B with bulk Nd. The mixed powders of 50 at.% Fe and 50 at.% B were first compressed under the pressure of 8 MPa, and then melted in a high frequency induction melting furnace under high-purity argon. Bulk Nd and $Fe_{50}B_{50}$ alloy annealed at 1223 K for 120 h in the evacuated quartz tube were melted in the arc furnace. It should be pointed out that the each Nd-Fe-B alloy sample (about 3 g) prepared by the two methods mentioned above was re-melted at least four times in order to ensure compositional homogeneity. The mass loss of the ingot was generally less than 1%.

Alloy samples were sealed into evacuated quartz and annealed (873 K for 1440 h, 1073 K for 960 h) and quenched in ice water. After that, powder samples were analyzed using x-ray diffraction techniques (PLXcel 3D, Co Kα radiation) in the range from 20° to 90°, 2θ with 0.2626 step sizes at 45 kV and 40 mA. The microstructures of alloy samples were examined by scanning electron microscopy (SEM) with energy dispersive spectrometry (EDS). The crystal structures of the phases in the alloys were characterized using Jade 6.5, X'Pert Highscore plus and Fullprof software.

4. Results and Discussions

The representative XRD patterns and backscattered electron (BSE) images of Nd-Fe-B alloys ($Nd_{15}Fe_{82.5}B_{2.5}$, $Nd_5Fe_{65}B_{30}$, $Nd_{15}Fe_{35}B_{50}$ and $Nd_{10}Fe_{20}B_{70}$) annealed at 873 K for 1440 h and alloys ($Nd_{7.5}Fe_{90}B_{2.5}$, $Nd_{25}Fe_{72.5}B_{2.5}$ and $Nd_{25}Fe_{60}B_{15}$) annealed at 1073 K for 960 h were analyzed and shown, respectively. It should be pointed out that the compositions of Nd and Fe in Nd-Fe-B alloys were shown in Tables 2 and 3, while those of B in Nd-Fe-B alloys were not given. The reason for it is that B as the light element could not be accurately measured quantitatively by EDS. The identified phases in Nd-Fe-B alloys by EDS are only based on the composition measured of Nd and Fe without consideration B content. In addition, the solubility of B in binary/ternary intermetallic compounds and solid solution phases could not be measured quantitatively in this work.

4.1 Phase Equilibria at 873 K

Figure 1(a) is the XRD pattern of $Nd_{7.5}Fe_{90}B_{2.5}$ alloy annealed at 873 K for 1440 h. As can be seen, the characteristic peaks of $Nd_2Fe_{14}B$ (τ_1), Nd_2Fe_{17} and Nd_5Fe_{17}

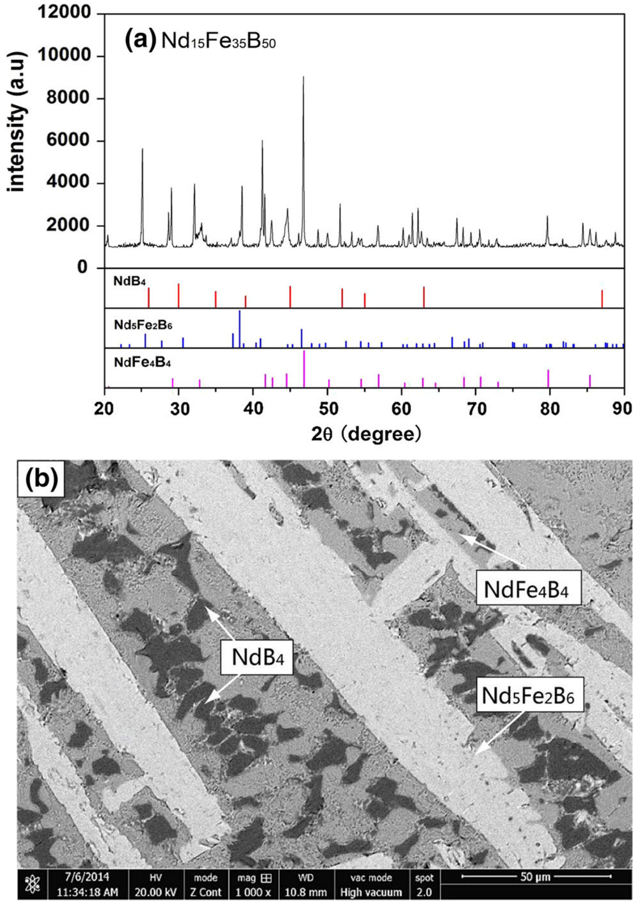

Fig. 3 XRD pattern and backscattered electrons (BSE) image of Nd15Fe35B50 alloy annealed at 873 K for 1440 h

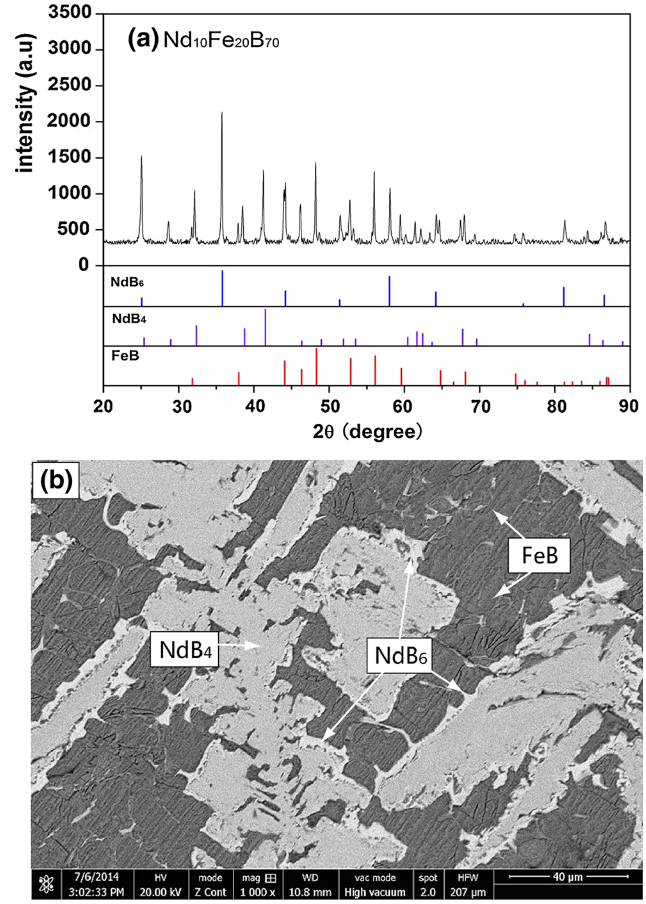

Fig. 4 XRD pattern and backscattered electrons (BSE) image of Nd10Fe20B70 alloy annealed at 873 K for 1440 h

phases are marked well. The ternary intermetallic compound, $Nd_2Fe_{14}B$ (τ_1), was determined to be $Nd_2Fe_{14}B$ structure with space group $P4_2/mnm$. Three-phase microstructure of this alloy is also observed in the back scattered electrons (BSE) image of the alloy in Fig. 1(b). Based on the EDS measurements, the compositions of the dark grey phase and the light grey phase are 11.23at.%Nd-88.77at.%Fe (Nd:Fe = 2:15.8) and 20.13at.%Nd-79.87at.%Fe (Nd:Fe = 5:19.8), respectively, which are corresponding to Nd_2Fe_{17} and Nd_5Fe_{17}. The white matrix phase with 13.24at.%Nd-86.76at.%Fe is approximately close to theoretical ratio (Nd:Fe = 2:14) and is identified as $Nd_2Fe_{14}B$ (τ_1). Therefore, the XRD results in $Nd_{7.5}Fe_{90}B_{2.5}$ alloy are in good agreement with the SEM/EDS examination.

As shown in Fig. 2(a), $Nd_5Fe_{67}B_{33}$ alloy is composed of three phases, $NdFe_4B_4$ (τ_2), Fe_2B and α-Fe, based on distinguished characteristic peaks of the XRD pattern. The ternary intermetallic compound, $NdFe_4B_4$ (τ_2), was determined to be $RE_{1.11}Fe_4B_4$ structure with space group Pccn. Figure 2(b) shows the three-phase microstructure of this alloy. From EDS results, the composition of the dark phase is 99.07at.%Fe-0.93at.%Nd, which is corresponding to α-Fe, and that of the grey matrix phase is 22.72at.%Nd-77.28at.%Fe, which is approximately close to theoretical ratio (Nd:Fe = 1:4) of $NdFe_4B_4$ (τ_2). The white phase in Fig. 2(b) is identified to be Fe_2B from the XRD analysis.

Figure 3(a) is the XRD pattern of $Nd_{15}Fe_{35}B_{50}$ alloy annealed at 873 K for 1440 h. It can be seen that the three phases, $NdFe_4B_4$ (τ_2), $Nd_5Fe_2B_6$ (τ_3) and NdB_4, are identified based on distinguished characteristic peaks of the XRD pattern. The ternary intermetallic compound, $Nd_5Fe_2B_6$ (τ_3), was determined to be $Pr_5Co_2B_6$ structure with space group R $\overline{3}$ m. Three-phase microstructure of the alloy is also observed in Fig. 3(b). According to the measured compositions by EDS, the composition of the grey matrix phase with 22.14at.%Nd-77. 86at.%Fe and the white phase as stripes with 69.78at.%Nd-30.22at.%Fe is approximately corresponding to theoretical ratios (Nd:Fe = 1:4 and Nd:Fe = 5:2) of $NdFe_4B_4$ (τ_2) and $Nd_5Fe_2B_6$(τ_3), respectively. The dark grey phase in Fig. 3(b) is considered to be NdB_4 on the basis of XRD analysis.

Figure 4(a) is the XRD pattern of $Nd_{10}Fe_{20}B_{70}$ alloy. The characteristic peaks of the three phases (NdB_4, NdB_6 and FeB) are well distinguished. Figure 4(b) is the BSE micrograph of the alloy, which shows three-phase microstructure. Due to the difficulty of quantitative measurements of content B in Nd-Fe-B alloys by EDS, it could

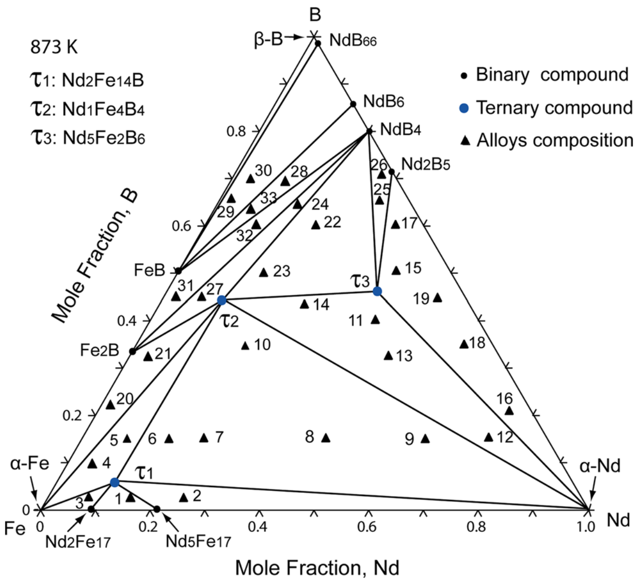

Fig. 5 Phase equilibria of the Nd-Fe-B ternary system at 873 K determined in this work. The three-phase equilibrium, NdB66 + FeB + β-B, was not found directly in the present experiments, but was concluded reasonably on the basis of the phase rule and the three-phase region, NdB6 + FeB + NdB66, which was determined from the XRD and SEM/EDS results of Nd2.5Fe32.5B65 and Nd2.5Fe27.5B70 alloys

still identify binary Nd-B compounds and binary Fe-B compounds only from the compositions of Nd and Fe in the different phases. In Fig. 4(b), the content of Fe in the dark grey phase is higher, while that of Nd in other color phases are much higher by EDS measurement. Combined with the XRD analysis in Fig. 4(a), the dark grey phase is identified to be FeB. On the other hand, although the grey phase and the light grey phase in Fig. 4(b) are impossible to be identified only by EDS results, the volume fraction of the grey phase is clearly much more compared with that of the light grey phase. Moreover, the nominal composition of $Nd_{10}Fe_{20}B_{70}$ alloy is closed to NdB_4. Therefore, the grey phase could be identified to be NdB_4, while the light grey phase would be NdB_6 according to the XRD analysis.

In this work, thirty-three Nd-Fe-B alloys annealed at 873 K for 1440 h were investigated and analyzed using the same method of the identified phases in four typical Nd-Fe-B alloys mentioned above. According to the experimental results as given in Table 2, the phase equilibria of the Nd-Fe-B ternary system at 873 K were constructed as shown in Fig. 5. It consists of 14 single-phase regions, 28 two-phase regions and 16 three-phase regions. It should be noticed that the three-phase equilibrium, NdB_{66} + FeB + β-B, was not found directly in the present experiments, but was concluded reasonably on the basis of the phase rule and the three-phase region, NdB_6 + FeB + NdB_{66}, which was determined from the XRD and SEM/EDS analysis of $Nd_{2.5}Fe_{32.5}B_{65}$ and $Nd_{2.5}Fe_{27.5}B_{70}$ alloys. On the other hand, compared with the isothermal section of the ternary system at 873 K reported by Chaban et al.,[5] it is obvious difference that Nd_5Fe_{17} with space group $P6_3/mcm$ was observed to be stable at 873 K in the present work, which is in agreement with the calculated results.[28] Meanwhile, $NdFe_2$ as a stable intermetallic compound reported by Chaban et al.[5] at 873 K was not found in the present experimental results and the calculated results.[28] In addition, ternary intermetallic compounds, $Nd_3Fe_{16}B$ and Nd_2FeB_3 denoted by Chaban et al.[5] were confirmed as $Nd_2Fe_{14}B$ (τ_1) and $Nd_5Fe_2B_6$(τ_3) in the present work, respectively, according to the experimental results.[36,45-47]

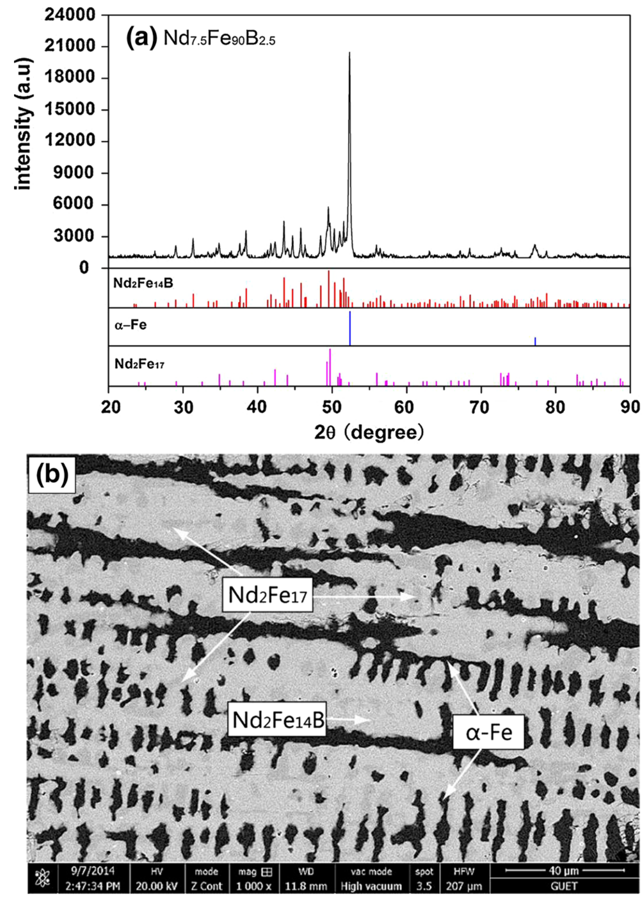

Fig. 6 XRD pattern and backscattered electrons (BSE) image of Nd7.5Fe90B2.5 alloy annealed at1073 K for 960 h

4.2 Phase Equilibria at 1073 K

Figure 6(a) indicates clearly the existence of three phases (α-Fe, Nd_2Fe_{17} and $Nd_2Fe_{14}B$) in $Nd_{7.5}Fe_{90}B_{2.5}$ alloy annealed at 1073 K for 960 h from the XRD pattern. The corresponding three-phase microstructure of this alloy is also shown in Fig. 6(b). According to EDS measurements, the compositions of the dark phase and dark grey phase are 98.84at.%Fe-1.16at.%Nd and 89.47at.%Fe-10.53at.%Nd, respectively, which are α-Fe and Nd_2Fe_{17} without any solubility of B, and that of the white matrix phase with 13.27at.%Nd-86.73at.%Fe is approximately close to the theoretical ratio (Nd:Fe = 2:14) of $Nd_2Fe_{14}B$ (τ_1). The white matrix phase is thus identified to be $Nd_2Fe_{14}B$ (τ_1).

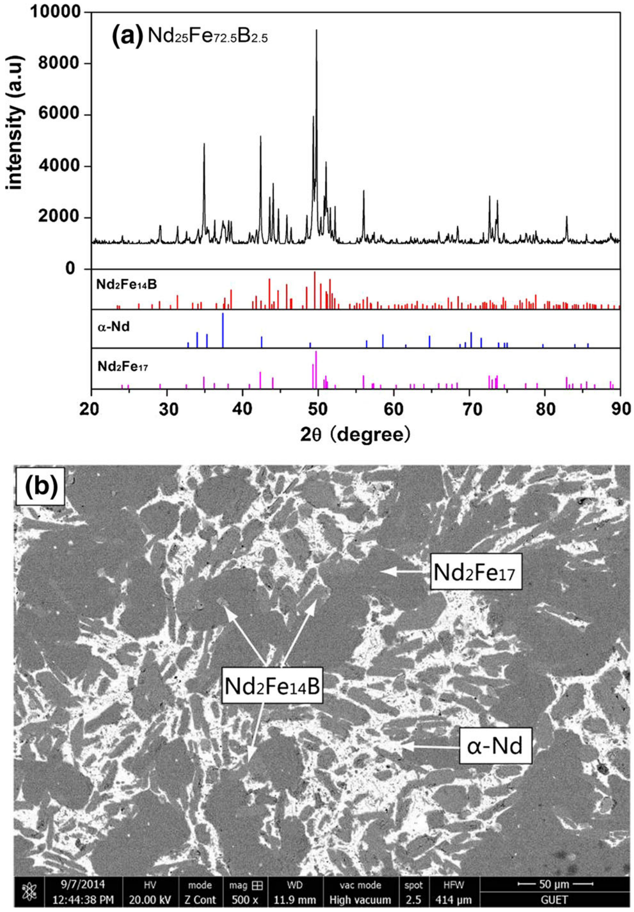

Fig. 7 XRD pattern and backscattered electrons (BSE) image of Nd25Fe72.5B2.5 alloy annealed at 1073 K for 960 h

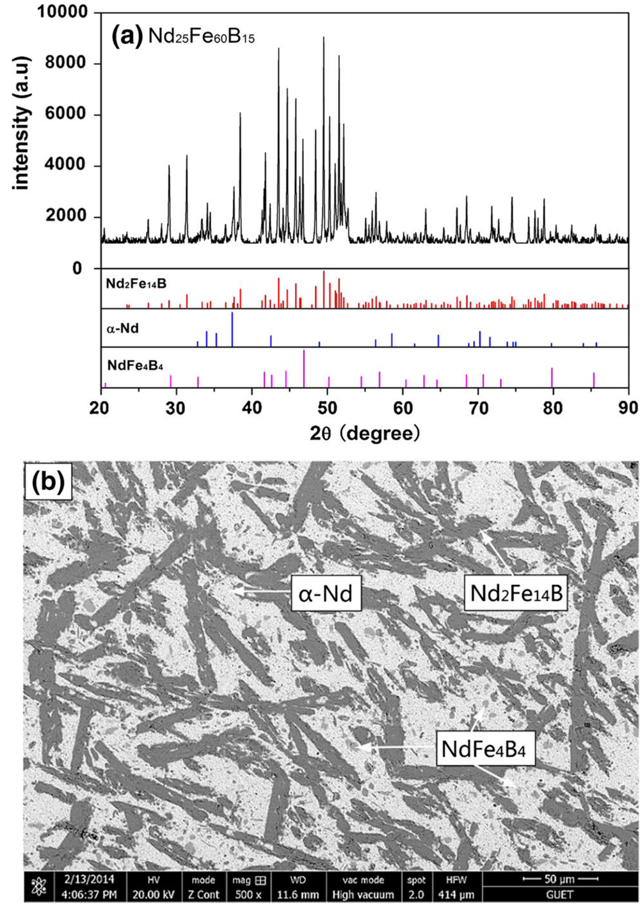

Fig. 8 XRD pattern and backscattered electrons (BSE) image of Nd25Fe60B15 alloy annealed at 1073 K for 960 h

Figure 7(a) is the XRD pattern of $Nd_{25}Fe_{72.5}B_{2.5}$ alloy annealed at 1073 K for 960 h. It can be seen that the three phases, Nd_2Fe_{17}, α-Nd and $Nd_2Fe_{14}B$ are identified based on distinguished characteristic peaks. The three-phase microstructure is identified from SEM results in Fig. 7(b). Based on EDS results, the compositions of the dark grey phase and the white phase are 11.43at.%Nd-88.57at.%Fe and 98.51at.%Nd-1.49at.%Fe, which are closed to Nd_2Fe_{17} and α-Nd without any solubility of B, respectively. The composition (14.21at.%Fe-85.79at.%Nd) of the light grey phase is considered to be $Nd_2Fe_{14}B$ (τ_1) according to the same analysis of identified phases in $Nd_{7.5}Fe_{90}B_{2.5}$ alloy.

$Nd_{25}Fe_{60}B_{15}$ alloy consists of three phases, $Nd_2Fe_{14}B$ (τ_1), $NdFe_4B_4$ (τ_2) and α-Nd by the XRD pattern analysis as shown in Fig. 8(a), while the BSE micrograph of the microstructure (three-phase) was also given in Fig. 8(b). According to the measured compositions by EDS, the compositions of the dark grey phase with 14.11at.%Nd-85.89at.%Fe and the light grey phase with 23.22at.%Nd-76.78. 22 at.% Fe are approximately corresponding to theoretical ratio (Nd:Fe = 2:14 and Nd:Fe = 1:4) of $Nd_2Fe_{14}B$ (τ_1) and $NdFe_4B_4$ (τ_2), respectively. The composition of the white phase is 99.82at.%Nd-0.18at.%Fe, which is closed to α-Nd.

In the present work, nineteen Nd-Fe-B alloys annealed at 1073 K for 960 h were investigated by XRD and SEM/EDS. Using same analysis of identified phases in three Nd-Fe-B alloys mentioned above, the determined experimental results were summarized in Table 3. Based on the phase relationships of nineteen Nd-Fe-B alloys, the phase equilibria of the Nd-Fe-B ternary system (excluding the B-rich part) at 1073 K was constructed as shown in Fig. 9. As can be seen, it consists of 8 single-phase regions, 14 two-phase regions and 7 three-phase regions in the Nd-Fe-rich field investigated in the present work. In addition, it is indicated that some Nd-Fe-B alloys studied in the present work could appear liquid phase at 1073 K according to the Nd-Fe binary system revised by Hallemans et al.[48] However, as shown from XRD patterns and BSE images of Nd-Fe-B alloys (seen in Fig. 6 and 8), liquid phase in alloy samples is impossible to be observed and α-Nd as the solid phase was found. The possible reason for it is the result of the solidification of liquid phase in alloy samples during quenched process after annealed at 1073 K. Based on the EDS/XRD results, the phase equilibria between liquid phase (α-Nd) and other phases were shown using dotted lines in Fig. 9. It should be also noted that the binary intermetallic compound Nd_5Fe_{17} was not found to be stable at 1073 K

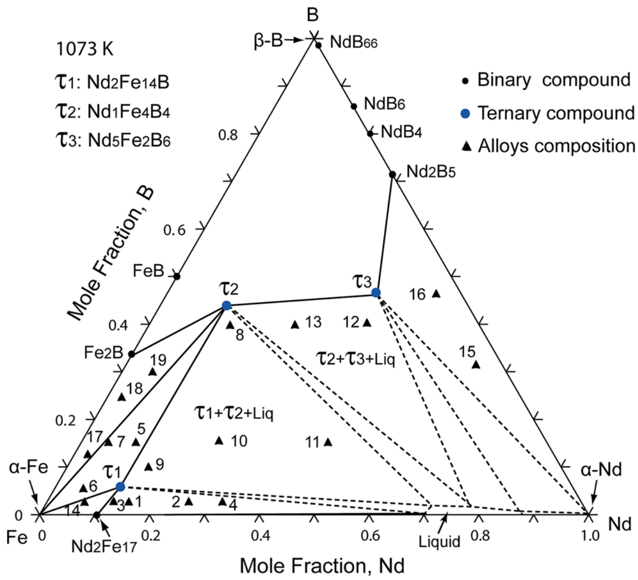

Fig. 9 Phase equilibria of the Nd-Fe-B ternary system at 1073 K determined in this work. Note that liquid phase in the alloy samples is impossible to be observed and α-Nd as the solid phase was found only. Liquid phase would transform to the solid phase (α-Nd) during the solidification in the process of quenching quickly alloy samples into ice water. The phase equilibria related to liquid phase were not measured directly and thus were used dotted lines to show three-phase regions determined, liquid + Nd_2Fe_{17} + $Nd_2Fe_{14}B$ (τ_1), liquid + $Nd_2Fe_{14}B$ (τ_1) + $NdFe_4B_4$ (τ_2), liquid + $NdFe_4B_4$ (τ_2) + $Nd_5Fe_2B_6$ (τ_3). In addition, the phase boundary of liquid phase was not measured in this work

according to the present experimental results as shown in Table 3.

5. Conclusions

On the basis of the microstructure examination and phase analysis of Nd-Fe-B alloys at 873 and 1073 K using XRD and SEM/EDS, the following conclusions in this work could be drawn:

(1) The phase equilibria of the Nd-Fe-B ternary system at 873 K in the whole compositional range and 1073 K in the Nd-Fe-rich part were constructed based on the XRD and SEM/EDS results. The experimental results show phase equilibria of the Nd-Fe-B ternary system at 873 K consists of 14 single-phase regions, 28 two-phase regions and 16 three-phase regions, while there are 8 single-phase regions, 14 two-phase regions and 7 three-phase regions at 1073 K except for the B-rich part.

(2) The ternary intermetallic compound, $Nd_2Fe_{14}B$ with space group $P4_2/mnm$ as $Nd_2Fe_{14}B$ structure type, $NdFe_4B_4$ with space group Pccn as $RE_{1.11}Fe_4B_4$ structure type and $Nd_5Fe_2B_6$ with space group R $\overline{3}$ m as $Pr_5Co_2B_6$ structure type were confirmed. In addition, Nd_2Fe_{17} and Nd_5Fe_{17} are stable at 873 K, while Nd_5Fe_{17} was not found at 1073 K in the present experiments.

Acknowledgments

This work was supported by National Basic Foundation of China (Grant No. 2014CB643703), Guangxi Natural Science Foundation (Grant Nos. 2014GXNSFBA118235, 2013GXNSFCA019017, 2012GXNSFGA060002) and Guangxi Key Laboratory of Information Materials, Guilin University of Electronic Technology, China (Grant No. 1210908-216-Z). The authors also acknowledge National Natural Science Foundation of China (Grant No. 51461013) for financial support.

References

1. M. Sagawa, S. Fujimura, N. Togawa, H. Yamamoto, and Y. Matsuura, New Material for Permanent Magnets on a Base of Nd and Fe, *J. Appl. Phys.*, 1984, **55**, p 2083-2087
2. S. Guo, Y.H. Liu, B.C. Chen, C.J. Yan, R.J. Chen, D. Lee, and A. Yan, Effect of Hydriding Degree on the Microstructure and Magnetic Properties of Sintered NdFeB Magnets, *J. Appl. Phys.*, 2012, **111**, p 827-831
3. S. Sugimoto, Current Status and Recent Topics of Rare-Earth Permanent Magnets, *J. Phys. Appl. Phys.*, 2011, **44**, p 110-118
4. N. Poudyal and J.P. Liu, Advances in Nanostructured Permanent Magnets Research, *J. Phys. Appl. Phys.*, 2012, **46**, p 43001-43023
5. N.F. Chaban, Yu.B. Kuz'ma, N.S. Bilonizhko, O.O. Kachmar, and N.V. Petrov, Ternary (Nd, Sm, Gd)-Fe-B Systems, *Dopov. Akad. Nauk URSR Ser. A Fit. Mat. Tekh. Nauki.*, 1979, 10, p 873-876
6. K. Loëwe, C. Brombacher, M. Katterb, and O. Gutfleisch, Temperature Dependent Dy Diffusion Processes in Nd-Fe-B Permanent Magnets, *Acta Mater.*, 2015, **83**, p 248-255
7. O. Gutfleisch, M.A. Willard, E. Brück, C.H. Chen, S.G. Sankar, and J.P. Liu, Magnetic Materials and Devices for the 21st Century: Stronger, Lighter, and More Energy Efficient, *Adv. Mater.*, 2011, **23**, p 821-842
8. H. Nakamura, K. Hirota, T. Ohashi, and T. Minowa, Coercivity Distributions in Nd-Fe-B Sintered Magnets Produced by the Grain Boundary Diffusion Process, *J. Phys. Appl. Phys.*, 2011, **44**, p 540-545
9. M. Sagawa, S. Hirosawa, H. Yamamoto, S. Fujimura, and Y. Matsuura, Nd-Fe-B Permanent Magnet Materials, *Jpn. J. Appl. Phys.*, 1987, **26**, p 785-800
10. T.H. Kim, S.R. Lee, S. Namkumg, and T.S. Jang, A Study on the Nd-Rich Phase Evolution in the Nd-Fe-B Sintered Magnet and Its Mechanism During Post-sintering Annealing, *J. Alloys Compd.*, 2012, **537**, p 261-268
11. K. Kobayashi, K. Urushibata, T. Matsushita, S. Sakamoto, and S. Suzuki, Magnetic Properties and Domain Structures in Nd-Fe-B Sintered Magnets with Tb Additive Reacted and Diffused from the Sample Surface, *J. Alloys Compd.*, 2014, **615**, p 569-575
12. C.D. Fuerst, T.W. Capehart, F.E. Pinkerton, and J.F. Herbst, Preparation and Characterization of $La_{2-x}Ce_xFe_{14}B$ Compounds, *J. Magn. Magn. Mater.*, 1995, **139**, p 359-363

13. W.F. Li, H.S. Amin, T. Ohkubo, N. Hase, and K. Hono, Distribution of Dy in High-Coercivity (Nd, Dy)-Fe-B Sintered Magnet, *Acta Mater.*, 2011, **59**, p 3061-3069
14. J.W. Kim, S.H. Kim, S.Y. Song, and Y.D. Kim, Nd-Fe-B Permanent Magnets Fabricated by Low Temperature Sintering Process, *J. Alloys Compd.*, 2013, **551**, p 180-184
15. Z.H. Hu, F.Z. Lian, M.G. Zhu, and W. Li, Effect of Tb on the Intrinsic Coercivity and Impact Toughness of Sintered Nd-Dy-Fe-B Magnets, *J. Magn. Magn. Mater.*, 2008, **320**, p 1735-1738
16. F. Vial, F. Joly, E. Nevalainen, M. Sagawa, K. Hiraga, and K.T. Park, Improvement of Coercivity of Sintered NdFeB Permanent magnets by Heat Treatment, *J. Magn. Magn. Mater.*, 2002, **1329**, p 242-245
17. J. Fidler, T. Schrefl, S. Sasaki, and D. Suess, The Role of Intergranular Regions in Sintered Nd-Fe-B Magnets with $(BH)_{max} < 420$ kJ m^3 (52.5 MGOe), *Jpn. Inst. Met.*, 2000, **14**, p S45-S54
18. L. Liang, M.Y. Wu, L.H. Liu, C. Ma, J. Wang, J.D. Zhang, and L.T. Zhang, Sensitivity of Coercivity and Squareness Factor of a Nd-Fe-B Sintered Magnet on Post-sintering Annealing Temperature, *J. Rare Earths*, 2015, **33**, p 507-513
19. W.F. Li, Ohkubo, and K. Hono, Effect of Post-sinter Annealing on the Coercivity and Microstructure of Nd-Fe-B Permanent Magnets, *Acta Mater.*, 2009, **57**, p 1337-1346
20. F.G. Chen, T.Q. Zhang, J. Wang, L.T. Zhang, and G.F. Zhou, Investigation of Domain Wall Pinning Effect Induced by Annealing Stress in Sintered Nd-Fe-B Magnet, *J. Alloys Compd.*, 2015, **640**, p 371-375
21. T.B. Massalski, H. Okamoto, P.R. Subramanian, and L. Kacprzak, *Binary Alloy Phase Diagrams*, ASM International, Materials Park, 1990
22. W. Zhang, G. Liu, and K. Han, The Fe-Nd (Iron-Neodymium) System, *J. Phase Equilib.*, 1992, **13**, p 645-648
23. A.M. Gabay, A.G. Popov, V.S. Belozerov, and A.S. Yermolenko, The Structure and Magnetic Properties of Rapidly Quenched and Annealed Multi-phase Nanocrystalline $Nd_9Fe_{91-x}B_x$, Ribbons, *J. Alloys Compd.*, 1996, **245**, p 119-124
24. F.J.G. Landgraf, G.S. Schneider, V. Villas-Boas, and F.P. Missell, Solidification and Solid State Transformations in Fe-Nd: A Revised Phase Diagram, *J. Less Commom Met.*, 1990, **163**, p 209-218
25. H. Okamoto, Fe-Nd (Iron-Neodymium), *J. Phase Equilib.*, 1997, **18**, p 106-106
26. J.M. Moreau, L. Paccard, J.P. Nozieres, F.P. Missel, G.S. Schneider, and V. Villas-Boas, A New Phase in the Nd-Fe System: Crystal structure of Nd_5Fe_{17}, *J. Less-Commom Met.*, 1990, **163**, p 245-251
27. C. Lin, C.X. Liu, Y.X. Sun, Z.X. Liu, D.F. Chen, C. Gou, K. Sun, and J.L. Yang, Neutron Diffraction Study of Nd_5Fe_{17}, *J. Magn. Magn. Mater.*, 1998, **186**, p 129-134
28. M.A.V. Ende and I.H. Jung, Critical Thermodynamic Evaluation and Optimization of the Fe-B, Fe-Nd, B-Nd and Nd-Fe-B Systems, *J. Alloys Compd.*, 2013, **548**, p 133-154
29. K.I. Portnoi, M.K. Levinskaya, and V.M. Romashov, Constitution Diagram of the System Iron-Boron, *Sov. Powder Metall. Met. Geram.*, 1969, **8**, p 657-659
30. P.K. Liao, K.E. Spear, and M.E. Schlesinger, The B-Nd (Boron-Neodymium) System, *J. Phase Equilib.*, 1996, **17**, p 335-339
31. H.A. Eick and P.W. Gilles, Precise Lattice Parameters of Selected Rare Earth Tetra-and Hexa-Borides, *J. Am. Chem. Soc.*, 1959, **81**, p 5030-5032
32. J. Roger, V. Babizhetskyy, R. Jardin, J.F. Halet, and R. Guérin, Solid State Phase Equilibria in the Ternary Nd-Si-B System at 1270 K, *J. Alloys Compd.*, 2006, **415**, p 73-84
33. E.K. Storm, Phase Relationship, Vaporization, and Thermodynamic Properties of Neodymium Hexaboride, *J. Phys. Chem.*, 1981, **85**, p 1536-1540
34. K.H.J. Buschow, New Permanent Magent Materials, *Mater. Sci. Rep.*, 1986, **1**, p 1-64
35. K.H.J. Buschow, D.B. de Mooij, and H.M. Van Noort, The Fe-Rich Isothermal Section of Nd-Fe-B at 900 °C, *Philips J. Res.*, 1985, **40**, p 227-238
36. G. Schneider, ETh Heing, G. Petzow, and H.H. Stadelmaier, Phase Relations in the Fe-Nd-B System, *Z. Metallkd.*, 1986, **77**, p 755-761
37. J.F. Herbst, J.J. Croat, and F.E. Pinkerton, Relationships Between Crystal Structure and Magnetic Properties, *Phys. Rev. B*, 1986, **29**, p 4176-4178
38. N. Zhang and Y. Luo, Phase Diagram of Nd-Fe-B Ternary System, *Sci. Sin. Ser. B*, 1989, **5**, p 329-332
39. G.C. Che and J.K. Liang, Phase Diagram of Nd-Fe-B Ternary System, *Sci. Sin. A*, 1986, **29**, p 1172-1185
40. V. Raghavan, The B-Fe-Nd (Boron-Iron-Neodymium) System, *Phase Diagrams of Ternary Iron Alloys,* Part 6A, Ind. Inst. Metals, Calcutta, 1992, p 374-386
41. A. Malfliet, G. Cacciamani, N. Lebrun, and P. Rogl, *Boron-Iron-Neodymium. Iron System, Part 1*, Springer, Berlin, 2008, p 482-511
42. K.G. Knoch, B. Reinsch, and G. Peztow, $Nd_2Fe_{14}B$ Its Region of Primary Solidification, *Z. Metallkd.*, 1994, **85**, p 350-353
43. F.J.G. Landgraf, F.P. Missell, G. Knoch, B. Grieb, and E.T. Heing, Binary Fe-Nd Metastable Phase in the Solidification of Fe-Nd-B Alloys, *J. Appl. Phys.*, 1991, **70**, p 6107-6109
44. Y. Mastsuura, S. Hirosawa, H. Yamamoto, S. Fujimura, M. Sagawa, and K. Osamura, Phase Diagram of the Nd-Fe-B System, *Jpn. J. Appl. Phys.*, 1985, **24**, p 635-637
45. J.F. Herbst, J.J. Croat, and F.E. Pinkerton, Relationships Between Crystal Structure and Magnetic Properties, *Phys. Rev. B*, 1986, **29**, p 4176-4178
46. D. Divord and P. Tenaud, Refinement of the Crystal Structure of R1 + εFe4B4 Compounds (R = Nd, Gd), *J. Less-Common Met.*, 1986, **123**, p 109-116
47. D.B. De Mooij and K.H.J. Buschow, Note on the Structure and Composition of the B-rich Ternary Phase in the Nd-Fe-B System, *Philips J. Res.*, 1988, **43**, p 70-74
48. B. Hallemans, P. Wollants, and J.R. Roos, Thermodynamic Assessment of the Fe-Nd-B Phase Diagram, *J. Phase Equilib.*, 1995, **16**, p 137-149
49. V. Raghavan, B-Fe-Nd (Boron-Iron-Neodymium), *J. Phase Equilib.*, 2013, **34**, p 124-128
50. H. Werheit, U. Kuhlmann, M. Laux, and T. Lundstrom, Structural and Electronic Properties of Carbon-Doped ß-Rhombohedral Boron, *Phys. Status Solidi (b)*, 1993, **179**, p 489-511